

# A SEMI-ANALYTIC SOLUTION ON THE 1D $S_N$ TRANSPORT EQUATION BY DECOUPLING THE IN-SCATTERING OPERATOR

Anderson English and Zeyun Wu

Department of Nuclear and Mechanical Engineering  
Virginia Commonwealth University  
Biotech Center, 800 E. Leigh St, Richmond, VA 23938  
englisham@vcu.edu; zwu@vcu.edu

## ABSTRACT

In this paper, we develop a semi-analytical solution for the one-dimensional discrete-ordinate (i.e.,  $S_N$ ) neutron transport equation by decoupling the in-scattering source using method of eigenfunction expansion. Conventional source iteration (SI) methods are usually employed in solving the  $S_N$  transport equation because the angular flux for any direction in the  $S_N$  equation is coupled with all angular fluxes from the equation's within-group in-scattering source term. By using a linear transformation technique, we aim to decouple the in-scattering operator in the transport equation and seek an accelerated solution by precluding the SI procedure. As a preliminary attempt, the in-scattering operator is decoupled with eigenfunction expansion which leads to a series of modified  $S_N$  equations that can be readily solved analytically in each problem domain. A numerical example demonstrates the accuracy, efficiency and other advantageous features of the proposed solution. Eliminating source iteration would significantly increase computational speed, however, the use of even-order Gauss-Legendre quadrature sets presents challenges in resolving the angular-spectra with unknown boundary conditions, even in the simple one-dimensional one-region slab-geometry case with vacuum boundaries. Our proposed solution requires iteration to find the angular-flux components at the region boundaries. As finer nodal-meshes degrade the convergence time of the previously mentioned iterative solutions, this drawback is relatively insignificant so long as the quadrature order is minimized.

*Key Words:* Transport, Scattering Operator, Discrete Ordinate

## 1. INTRODUCTION

With standard notations, the one-dimensional multigroup discrete-ordinate (i.e.,  $S_N$ )  $k$ -eigenvalue transport equation is described as

$$\begin{aligned} \mu_m \frac{\partial \psi_{mg}(x)}{\partial x} + \Sigma_{tg}(x) \psi_{mg}(x) = & \sum_{l=0}^L \frac{2l+1}{2} \Sigma_{sl, g \rightarrow g}(x) P_l(\mu_m) \phi_{lg}(x) \\ & + \sum_{\substack{g'=1 \\ g' \neq g}}^G \sum_{l=0}^L \frac{2l+1}{2} \Sigma_{sl, g' \rightarrow g}(x) P_l(\mu_m) \phi_{lg'}(x) + \frac{1}{k} \frac{\chi_g}{2} \sum_{g'=1}^G \nu \Sigma_{fg'}(x) \phi_{0g'}(x) \end{aligned}, \quad (1)$$

where the  $l^{\text{th}}$  angular flux moment  $\phi_{lg}(x)$  is given by

$$\phi_{lg}(x) = \sum_{m'=1}^N w_{m'} P_l(\mu_{m'}) \psi_{m'g}(x) . \quad (2)$$

The group-to-group scattering source and fission source can be assumed to be a known quantity under the framework of power iteration method in the  $k$ -eigenvalue transport solver. Thus, the remaining focus would be to solve the flux at group  $g$ , if we denote

$$S_g(x) = \sum_{\substack{g'=1 \\ g' \neq g}}^G \sum_{l=0}^L \frac{2l+1}{2} \Sigma_{sl, g' \rightarrow g}(x) P_l(\mu_m) \phi_{lg'}(x) + \frac{1}{k} \frac{\chi_g}{2} \sum_{g'=1}^G \nu \Sigma_{fg'}(x) \phi_{0g'}(x), \quad (3)$$

Eq. (1) is reduced to

$$\mu_m \frac{\partial \psi_{mg}(x)}{\partial x} + \Sigma_{tg}(x) \psi_{mg}(x) = \sum_{l=0}^L \frac{2l+1}{2} \Sigma_{sl, g \rightarrow g}(x) P_l(\mu_m) \phi_{lg}(x) + S_g(x). \quad (4)$$

As indicated in Eq.(2), the flux moment (if  $l = 0$ , it became the group scalar flux) appearing in the scattering source term is constructed with angular fluxes of all direction. Because of this angular flux coupling, Eq.(4) is commonly solved with the source iteration (SI) technique, which sometimes is very slow to converge. Here we propose a linear transformation technique that can decouple the within-group in-scattering operator from Eq.(4) and yield equations only involving individual angular components. By working this way, the conventional time-consuming source iteration process can be completely eliminated. Furthermore, the resulting equation produces accurate solutions without any spatial discretization errors and can be solved efficiently with analytical techniques.

## 2. LINEAR TRANSFORMATION OF THE SOURCE PROBLEM

Whilst deriving the proposed equations simply yet generously, we consider the  $S_N$  transport equation with the angular flux moment only up to  $l=1$ ,

$$\mu_m \frac{\partial \psi_{mg}(x)}{\partial x} + \Sigma_{tg}(x) \psi_{mg}(x) = \frac{1}{2} \Sigma_{s0, g \rightarrow g}(x) \phi_{0g}(x) + \frac{3}{2} \Sigma_{s1, g \rightarrow g}(x) \mu_m \phi_{1g}(x) + S_g(x). \quad (5)$$

where

$$\phi_{0g}(x) = \sum_{m'=1}^N w_{m'} \psi_{m'g}(x), \quad \phi_{1g}(x) = \sum_{m'=1}^N w_{m'} \mu_{m'} \psi_{m'g}(x). \quad (6)$$

For brevity, we drop off the subscript  $g$  for the energy group, and simplify the equation to a one-group formulation as follows

$$\mu_m \frac{\partial \psi_m(x)}{\partial x} + \Sigma_t(x) \psi_m(x) = \frac{1}{2} \Sigma_{s0}(x) \sum_{m'=1}^N w_{m'} \psi_{m'}(x) + \frac{3}{2} \Sigma_{s1}(x) \mu_m \sum_{m'=1}^N w_{m'} \mu_{m'} \psi_{m'}(x) + S(x), \quad m = 1, \dots, N. \quad (7)$$

Here we emphasize the equation only represents angular flux in one direction by showing the total number of the equations is  $N$  - the number of quadrature sets used in the  $S_N$  method.

Assuming homogeneous material in a cell  $i$  within the domain  $x_{i-1/2} < x < x_{i+1/2}$ , we may write the  $S_N$  transport equation in the cell as

$$\mu_m \frac{\partial \psi_m(x)}{\partial x} + \Sigma_t^i \psi_m(x) = \frac{1}{2} \Sigma_{s0}^i \sum_{m'=1}^N w_{m'} \psi_{m'}(x) + \frac{3}{2} \Sigma_{s1}^i \mu_m \sum_{m'=1}^N w_{m'} \mu_{m'} \psi_{m'}(x) + S(x), \quad m = 1, \dots, N \quad (8)$$

Eq.(8) can be re-written as

$$\frac{\partial \psi_m(x)}{\partial x} + \frac{\Sigma_t^i}{\mu_m} \psi_m(x) = \frac{1}{\mu_m} \left[ \frac{1}{2} \Sigma_{s0}^i \sum_{m'=1}^N w_{m'} \psi_{m'}(x) + \frac{3}{2} \Sigma_{s1}^i \mu_m \sum_{m'=1}^N w_{m'} \mu_{m'} \psi_{m'}(x) + S(x) \right], \quad m = 1, \dots, N \quad (9)$$

If we write the angular flux of all  $S_N$  directions into a vector with the dimension  $N$ ,

$$\boldsymbol{\Psi}(x) = \begin{bmatrix} \psi_1(x) \\ \psi_2(x) \\ \vdots \\ \psi_N(x) \end{bmatrix}. \quad (10)$$

Eq.(9) can be expressed as a matrix form as follows

$$\frac{\partial \boldsymbol{\Psi}(x)}{\partial x} + \mathbf{A}^i \boldsymbol{\Psi}(x) = S(x) \mathbf{b}, \quad (11)$$

where the vector  $\mathbf{b}$  is

$$\mathbf{b} = \begin{bmatrix} 1/\mu_1 \\ 1/\mu_2 \\ \vdots \\ 1/\mu_N \end{bmatrix}, \quad (12)$$

and the coefficient matrix  $\mathbf{A}^i$  appeared in Eq.(11) is associated with cell  $i$  and represents

$$\mathbf{A}^i = \begin{bmatrix} \frac{1}{\mu_1} \left( \Sigma_t^i - \frac{1}{2} \Sigma_{s0}^i w_1 - \frac{3}{2} \Sigma_{s1}^i \mu_1 w_1 \mu_1 \right) & -\frac{1}{\mu_1} \left( \frac{1}{2} \Sigma_{s0}^i w_2 + \frac{3}{2} \Sigma_{s1}^i \mu_1 w_2 \mu_2 \right) & \cdots & -\frac{1}{\mu_1} \left( \frac{1}{2} \Sigma_{s0}^i w_N + \frac{3}{2} \Sigma_{s1}^i \mu_1 w_N \mu_N \right) \\ -\frac{1}{\mu_2} \left( \frac{1}{2} \Sigma_{s0}^i w_1 + \frac{3}{2} \Sigma_{s1}^i \mu_2 w_1 \mu_1 \right) & \frac{1}{\mu_2} \left( \Sigma_t^i - \frac{1}{2} \Sigma_{s0}^i w_2 - \frac{3}{2} \Sigma_{s1}^i \mu_2 w_2 \mu_2 \right) & \vdots & -\frac{1}{\mu_2} \left( \frac{1}{2} \Sigma_{s0}^i w_N + \frac{3}{2} \Sigma_{s1}^i \mu_2 w_N \mu_N \right) \\ \vdots & \vdots & \ddots & \vdots \\ -\frac{1}{\mu_N} \left( \frac{1}{2} \Sigma_{s0}^i w_1 + \frac{3}{2} \Sigma_{s1}^i \mu_N w_1 \mu_1 \right) & -\frac{1}{\mu_N} \left( \frac{1}{2} \Sigma_{s0}^i w_2 + \frac{3}{2} \Sigma_{s1}^i \mu_N w_2 \mu_2 \right) & \cdots & \frac{1}{\mu_N} \left( \Sigma_t^i - \frac{1}{2} \Sigma_{s0}^i w_N - \frac{3}{2} \Sigma_{s1}^i \mu_N w_N \mu_N \right) \end{bmatrix}$$

The basic idea of decoupling the scattering operator is to linearly transform the angular flux into the eigenfunction space of the  $N \times N$  coefficient matrix  $\mathbf{A}^i$ . Assuming the eigen-vectors of  $\mathbf{A}^i$  are  $\mathbf{u}_m$  ( $m = 1, \dots, N$ ) with the associated eigenvalue  $\lambda_m$  so that

$$\mathbf{A}^i \mathbf{u}_m = \lambda_m \mathbf{u}_m \quad (m = 1, \dots, N), \quad (13)$$

One can express the angular flux vector  $\boldsymbol{\psi}(x)$  shown in Eq.(10) as a linear combination of  $\mathbf{u}_m$

$$\boldsymbol{\psi}(x) = \sum_{m=1}^N \varphi_m(x) \mathbf{u}_m, \quad (14)$$

Where the coefficients  $\varphi_m(x)$  are to be determined. The vector  $\mathbf{b}$  in the source term can also be expressed in the same manner

$$\mathbf{b} = \sum_{m=1}^N b_m \mathbf{u}_m. \quad (15)$$

By substituting Eq.(14) and (15) into Eq.(11), we arrive at the following equations

$$\sum_{m=1}^N \frac{\partial \varphi_m(x)}{\partial x} \mathbf{u}_m + \sum_{m=1}^N \varphi_m(x) \mathbf{A}^i \mathbf{u}_m = S(x) \sum_{m=1}^N b_m \mathbf{u}_m. \quad (16)$$

With a minor manipulation, the equations can be written into the following form

$$\sum_{m=1}^N \mathbf{u}_m \left[ \frac{\partial \varphi_m(x)}{\partial x} + \lambda_m \varphi_m(x) - b_m S(x) \right] = 0. \quad (17)$$

Since  $\mathbf{u}_m$  ( $m = 1, \dots, N$ ) are independent basis vectors of the eigen-space of the matrix  $\mathbf{A}^i$ , Eqs.(17) hold if and only if

$$\frac{\partial \varphi_m(x)}{\partial x} + \lambda_m \varphi_m(x) - b_m S(x) = 0 \quad \text{for } m = 1, \dots, N. \quad (18)$$

Eqs.(18) are the resulting decoupled equations, in which each individual equation is linked to its individual angular component and can be solved analytically. In the next section, we will discuss the procedure to obtain the solutions in Eq.(18) and demonstrate how these solution can be used to construct the real angular flux using Eq.(14).

### 3. ANALYTICAL SOLUTION

#### 3.1 Solving the Eq.(18) Analytically

Though the direction cosine  $\mu_m$  is not explicitly contained in the Eq.(18), to solve the equation analytically for a one-dimensional slab, we must consider the solutions for the  $\mu_m < 0$  and  $\mu_m > 0$  cases separately because different boundary condition may be imposed for each case. For simplicity, we truncate the proceeding equations by withholding the range for  $m$ . Rearranging Eq.(18) and applying an integrating factor  $e^{\lambda_m x}$  gives

$$d \left[ e^{\lambda_m x} \varphi_m(x) \right] = b_m S(x) e^{\lambda_m x} dx. \quad (19)$$

Next, we integrate from 0 to  $x$  ( $\mu_m > 0$ ), leaving

$$e^{\lambda_m x} \varphi_m(x) - \varphi_{mL} = \begin{cases} S_0 b_m \frac{1}{\lambda_m} (e^{\lambda_m x} - 1), & S(x) = S_0 \\ 0, & S(x) = 0 \end{cases}. \quad (20)$$

$\varphi_{mL}(x)$  is the boundary value at the leftmost cell-edge or any left hand sub-region interface, assuming  $+x$  is towards the right of the slab. Subscript  $R$  represents the right side. Note that the solution of Eq.(18),  $\varphi_m(x)$ , is not the ‘real’ angular flux for the problem; it has been dubbed the ‘fake’ angular flux due to satisfying the resulting modified transport equation and the linear transformation of scattering operator. The boundary values  $\varphi_{mL}(x)$  and  $\varphi_{mR}(x)$  are currently unknown due to their coupling with the angular flux, which has unknown incident components. We will discuss the solution methodology for the boundaries later in the section. For now, we treat them as knowns. The equations account for both a homogenous source term and a source-free region. Integrating from  $x$  to  $L$  ( $\mu_m < 0$ ) gives

$$e^{\lambda_m L} \varphi_{mR} - e^{\lambda_m x} \varphi_m(x) = \begin{cases} S_0 b_m \frac{1}{\lambda_m} (e^{\lambda_m L} - e^{\lambda_m x}), & S(x) = S_0 \\ 0, & S(x) = 0 \end{cases}, \quad (21)$$

where  $L$  is the total length of the slab, and  $\varphi_{mR}$  is the boundary value at the rightmost cell-edge or any right hand sub-region interface. Solving each equation for  $\varphi_m(x)$  in Eq. (20) and (21) yields the  $\varphi_m(x)$  solutions for  $\mu_m > 0$  and  $\mu_m < 0$  respectively

$$\varphi_m(x) = \begin{cases} \varphi_{mL} e^{-\lambda_m x} + \frac{S_0 b_m}{\lambda_m} (1 - e^{-\lambda_m x}), & S(x) = S_0 \\ \varphi_{m0} e^{-\lambda_m x}, & S(x) = 0 \end{cases} \quad (22)$$

$$\varphi_m(x) = \begin{cases} \frac{S_0 b_m}{\lambda_m} (1 - e^{\lambda_m(L-x)}) + \varphi_{mR} e^{\lambda_m(L-x)}, & S(x) = S_0 \\ \varphi_{mR} e^{\lambda_m(L-x)}, & S(x) = 0 \end{cases}. \quad (23)$$

Notice that the component variables are all known except for our boundary values, thus the analytic solutions for  $\varphi_m(x)$  are readily achieved assuming the boundary values are known.

### 3.2 Forming the scalar flux

Solving Eq.(18) for the ‘fake’ angular flux  $\varphi_m(x)$  is not our ultimate goal; we use it to form the angular flux  $\psi_m(x)$  and subsequently the scalar flux  $\phi(x)$ . Because the angular flux is a linear combination of the ‘fake’ angular flux and the eigenvector  $\mathbf{u}_m$  ( $m=1, \dots, N$ ) of matrix  $\mathbf{A}^i$  as seen in Eq.(14), it provides us a means to construct the angular flux solutions. We define the scalar flux at any point  $x$  using Eq.(6).

$$\phi(x) = \sum_{i=1}^N w_i \psi_i(x) \quad \text{for } i = 1, \dots, N \quad (24)$$

Because the combination of eigenvector  $\mathbf{u}_m$  with  $\varphi_m(x)$  requires specific matrix indexes, we denote the eigenvector component index as  $u_{im}$ , where  $i$  is the vector index corresponding to each quadrature value and  $m$  is the coupled vector to each eigenvalue. By combining Eq.(24) and Eq.(14), we get

$$\phi(x) = \sum_{i=1}^N w_i \left( \sum_{m=1}^N \varphi_m(x) u_{im} \right). \quad (25)$$

For simplicity, we introduce another region-dependent dummy variable  $w'_m$  to combine the constant eigenvectors and weight vector linearly so that

$$w'_m = \sum_{i=1}^N w_i u_{im}. \quad (26)$$

The scalar flux can now be simplified to

$$\phi(x) = \sum_{m=1}^N \varphi_m(x) w'_m \quad (27)$$

#### 4. IMPLEMENTATION AND THE BOUNDARY PROBLEM

The formation of the scalar flux from Eq. (27) is trivial using nested loops once all values of  $\varphi_m(x)$  are known. For any arbitrary number of sub-regions with different cross-section properties, the scattering operators and their corresponding eigenvectors, eigenvalues, and the values of  $\mathbf{b}$  (see Eq.(15)) can be found initially and stored with little cost. Note that normalization of the scattering operator eigenvectors is still accurate for this method.

To find the ‘fake’ angular flux, conventional transport sweeps can be applied in the directions  $\mu_m > 0$  then  $\mu_m < 0$ , respectively, calling the stored values when needed using the solutions in Eq.(22) and Eq.(23) depending on the inclusion of a source.

We discretize the regions into a nodal mesh of arbitrary density. To eliminate truncation errors, we work on the node centers. We now focus on how to find the unknown boundary conditions for the ‘fake’ angular flux at the slab boundaries.

##### 4.1 Iteration on the Boundaries

We named this decoupled scattering transformation a ‘semi-analytical’ (SA) method because the solution is still based on  $S_N$  transport formulation and requires an iterative loop to converge onto the complete boundary condition using a form of forward substitution. As a proof of feasibility of the proposed method, our code solved the problem for a one-region case with vacuum boundaries on each side of the slab, namely the incoming angular flux is zero at each side. Since the ‘fake’ angular flux is constructed from the real angular flux in the entire direction domain (see Eq.(14)), we make an initial guess for each unknown components of  $\boldsymbol{\psi}$  at the left and right vacuum boundaries as visualized in Fig. 1 below.

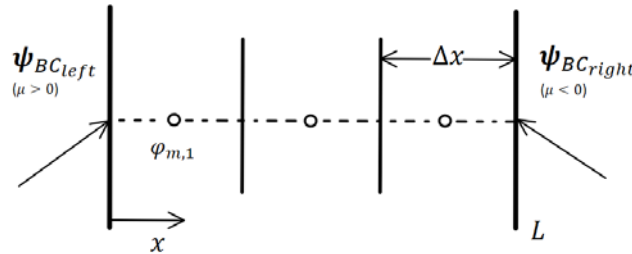


**Figure 1. Example mesh.**

We next decompose the vectors  $\boldsymbol{\psi}_{bc}$  at the left and right boundaries into their components of ‘fake’ angular flux using Eq.(14) so that  $\varphi_m(0) = \varphi_{mL}$  and  $\varphi_m(L) = \varphi_{mR}$ . The set of  $\varphi_{mL}$  and  $\varphi_{mR}$  are the initial boundary conditions to solve for  $\varphi_m(x)$  using the solutions in Eq.(22) and Eq.(23). We transport sweep to the right side vacuum boundary solving for the  $N/2$  values of  $\varphi_m(x)$  ( $\mu_m > 0$ ) at the node centers using Eq.(22); the number of points  $x$  depends on the selected node density. Once at the right boundary, we replace the values of  $\varphi_m(L)$  for  $\mu_m > 0$  with the values we just solved for. We now sweep from  $x = L$  back to  $x = 0$  for the other  $N/2$

values of  $\varphi_m(x)$  ( $\mu_m < 0$ ) using Eq.(22), executing the same replacement method as before, except now we apply the new values of  $\varphi_{mL}$  at the left boundary. After the one sweep, we can construct the angular flux using Eq.(14) at the boundaries, reapply the known values (zero for vacuum) and check the convergence. When forming the angular flux, the known incident flux components must be set to zero due to vacuum boundary conditions. We use relationship for the two-norm error of the two non-zero boundary angular flux vector components as the convergence criterion for the boundary angular flux

$$\varepsilon_{bc} = \left\| \frac{\Psi_{bc}^{(n+1)} - \Psi_{bc}^{(n)}}{\Psi_{bc}^{(n+1)}} \right\|_2, \quad (29)$$

Where  $(n)$  represents the older sweep. Once the values converge ( $\varepsilon \leq 10^{-6}$ , for our case), the angular flux and subsequently the scalar flux for every node can be calculated. If the flux is not converged, we decompose the boundary angular flux into their ‘fake’ phi components as before and repeat the process until the converged solutions are achieved.

## 5. NUMERICAL RESULTS

To evaluate the viability of our method, we compared the results from our method with the solutions yielded from the standard SI method with Diamond-Difference. A single region problem is considered with a total cross section of  $\Sigma_t = 2.0 [\text{cm}^{-1}]$ , a scattering ratio of  $c = 0.9$ , and a slab width of  $L = 20 [\text{cm}]$ . Vacuum boundaries are imposed on both sides. Constant external source is assumed everywhere in the region. Only an isotropic scattering source is considered at this time, but the method should be easily extended to the anisotropic scattering case. Fig. 2 depicts the flux results yielded from both methods.

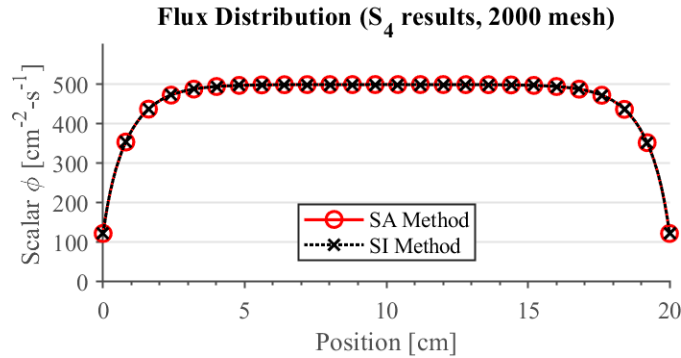


**Figure 2. Flux distribution.**

The relative two-norm error between the methods for a 2000 cell mesh is  $\epsilon = 4.041\text{E-}4$ , which indicates they are effectively identical solutions. Since the difference of the two results are essentially indistinguishable, it verifies the viability of the proposed method. However, noticeable error occurs approaching the boundaries. Fig. 3 provides zoomed plots of the relative error between the SI reference case and our SA method.

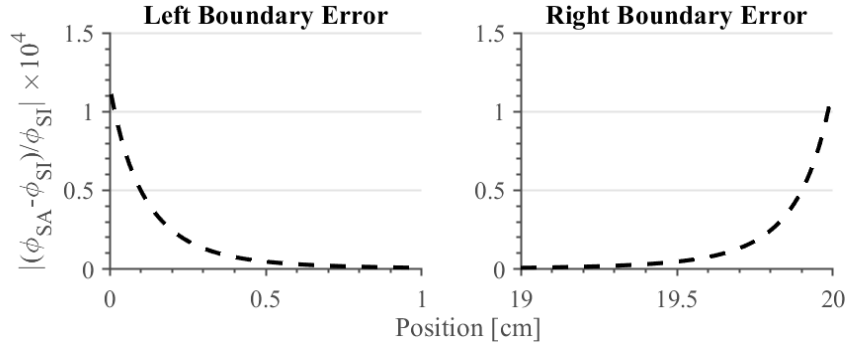


**Figure 3. Flux Discrepancy at Boundaries**

As our initial motivation of the semi-analytic solution is to reduce the computation cost by precluding the source iteration process in the transport solver, we checked how various scattering ratios effected the computation speed and iteration number for both methods with a mesh size of 2000. The data is presented in Table I.

**Table I. Computational results: speed of SA and SI methods**

Scattering Ratio $c$	SA Number	SA Time <sup>†</sup> [s]	SI Number	SI Time <sup>†</sup> [s]	Relative Error*
0.1	3	0.048	9	0.050	8.07E-04
0.5	6	0.067	26	0.095	6.69E-04
0.9	15	0.155	143	0.381	4.04E-04
0.95	32	0.223	275	0.616	3.27E-04
0.99			463	1.005	

<sup>†</sup> Computations on an Intel i7 7700K w/ 32GB DDR5 RAM

\* Relative 2-normalized error between SI and SA flux

As shown in the table, the SA method in general shows some computational cost reduction compared to the SI method. The total iteration number required for the boundary flux is consistently much less than the one needed in the SI procedure. At lower scattering ratios, the two methods require comparable time, but SA requires fewer iterations. For a scattering ratio  $c = 0.9$  or  $0.95$ , the speed advantages of our method are apparent. The method is between two to three times faster. However, we do not have a results comparison for  $c = 0.99$  at this stage because a negative angular flux is observed at the boundaries which eventually diverges the solution in this case. We are still working on this issue and hope the updated results will be available in the final paper. As our method essentially relies on analytic solutions for spatial variables, theoretically it should have no discretization errors in space. This salient feature of the proposed method is demonstrated with the results shown in Fig. 4.

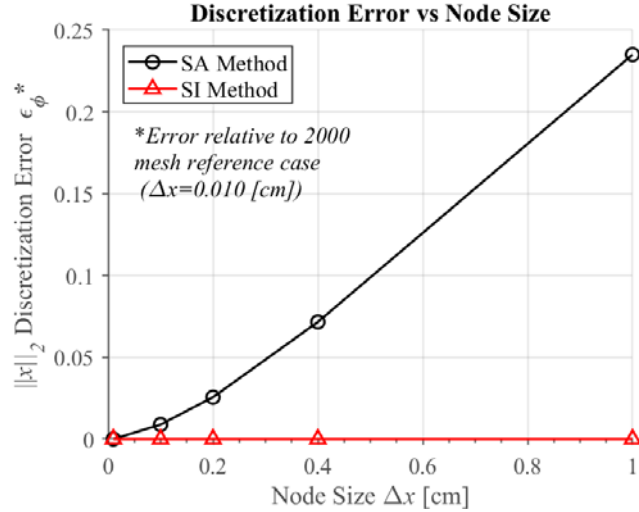


**Figure 4. Comparison of the spatial discretization errors.**

As can be seen, the truncation error due to spatial discretization increases significantly from the  $\Delta x = 0.01$  [cm] case to the  $\Delta x = 1.00$  case for the SI method, while for the SA case, the error is negligible for all different  $\Delta x$ ; it peaks at  $\epsilon = 8.362\text{E-}13$ . While the flux solution is normally found at the node centers in the code, to compare different node sizes, the cases with reduced node numbers must be a factor of 2000 and be additionally calculated then compared on node edges so that the positions overlap. The small error is likely caused by the final update of the left edge flux within the iteration, as the cell edge flux was calculated outside the iterative loop only after the final boundary flux values were found.

## 6. CONCLUSIONS

For the simple single-region case, the accuracy of the SA method is independent of truncation, and it is noticeably faster with scattering ratios up to  $c \approx 0.9$ . Another benefit of the SA method is that the iteration only occurs at the slab boundaries; the speed will be independent of the number of regions included in the problem, possibly apart from included vacuum regions.

Future additions to this project will include various boundary types and analysis of the multi-region scenario. Inclusion of a multi-region case will be potentially complicated; the interface values are dependent on the material properties of both adjacent regions. We will further extend the method to the multigroup formulation with general anisotropic scattering cross sections, and apply the method to  $k$ -eigenvalue problem as well.